

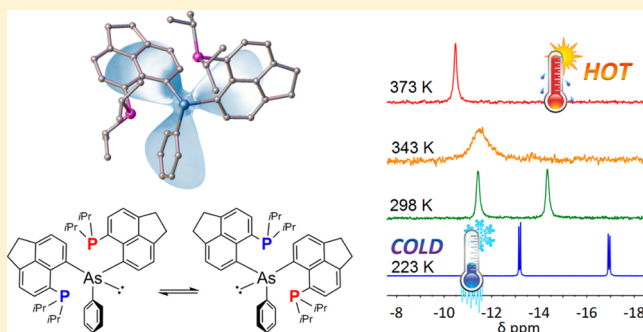
Geminally Substituted Tris(acenaphthyl) and Bis(acenaphthyl) Arsines, Stibines, and Bismuthine: A Structural and Nuclear Magnetic Resonance Investigation

Brian A. Chalmers, Christina B. E. Meigh, Phillip S. Nezman, Michael Bühl, Tomáš Lébl, J. Derek Woollins, Alexandra M. Z. Slawin, and Petr Kilian*

EaStChem School of Chemistry, University of St Andrews, St Andrews, Fife KY16 9ST, U.K.

Supporting Information

ABSTRACT: Tris(acenaphthyl)- and bis(acenaphthyl)-substituted pnictogens ($iPr_2P-Ace)_3E$ (**2–4**) ($E = As, Sb, \text{ or } Bi$; $Ace = \text{acenaphthene-5,6-diyl}$) and $(iPr_2P-Ace)_2EPh$ (**5 and 6**) ($E = As \text{ or } Sb$) were synthesized and fully characterized by multinuclear nuclear magnetic resonance (NMR), high-resolution mass spectrometry, elemental analysis, and single-crystal X-ray diffraction. The molecules adopt propeller-like geometries with the restricted rotational freedom of the sterically encumbered iPr_2P-Ace groups resulting in distinct NMR features. In the tris(acenaphthyl) species (**2–4**), the phosphorus atoms are isochronous in the $^{31}P\{^1H\}$ NMR spectra, and the rotation of the three acenaphthyl moieties around the $E-C_{ipso}$ bond is locked. On the other hand, the bis(acenaphthyl) species show a fluxional behavior, resulting in an A_X to A_2 spin system transition in the $^{31}P\{^1H\}$ variable-temperature NMR spectra. This allowed elucidation of remarkable through-space couplings ($^8J_{PP}$) of 11.5 Hz (for **5**) and 25.8 Hz (for **6**) at low temperatures. In addition, detailed line shape analysis of the thermodynamic parameters of the restricted rotation of the “propeller blades” in **5** was performed in the intermediate temperature region and also at coalescence. The lone pairs on the pnictogen atoms in **2–6** are oriented such that they form a bowl-shaped area that is somehow buried within the molecule.



INTRODUCTION

Tridentate phosphines have been described extensively in the literature, with the majority of the reports focusing on their use in catalysis.¹ As for other phosphines, the versatility of tridentate phosphines as ligands stems from the ability to manipulate the steric and electronic properties by varying the groups attached to the phosphorus donor atoms. In addition, flexibility of the linkages joining the donor atoms in multidentate ligands is also tunable. The rather flexible ligand, triphos (**A**) (Figure 1), is one of the most extensively studied tridentate phosphines as mentioned in a recent review by Ilia.^{2,3} Ligand **B** represents a less flexible tris(phosphine), with *ortho*-substituted phenyl linkages favoring metal chelation.⁴ On the other hand, tetradentate phosphines such as **C**,⁵ **D**,⁶ and **E**⁴ have been much less explored, often because of the challenging multistep synthesis involved. Coordination chemistry of these ligands is somehow complicated by the variety of coordination modes these ligands display, which makes their chemistry somehow less predictable. An example of this coordinative variety includes the bimetallic iron(II) complex **F** in which one tetrakis(phosphine) ligand **D** is coordinating in a bidentate mode, and the other in a tridentate mode to one metal atom and monodentate to the other.⁶ More rigid tetradentate phosphines also form bimetallic bidentate systems such as

complex **G**, which was obtained from the reaction of tetrakis(diphenylphosphino)-*p*-xylene with $Fe_2(CO)_9$.⁷

We have recently reported a synthetic and coordination study of the first geminally bis(*peri*-substituted) tridentate phosphine (**H**).⁸ It was synthesized by the reaction of **1** with $1/2$ equiv of $iPrPCL_2$, giving the tris(phosphine) in a respectable yield (68%). Tris(phosphine) **H** displayed complex variable-temperature (VT) nuclear magnetic resonance (NMR) behavior. At room temperature, a broad singlet was observed in the $^{31}P\{^1H\}$ NMR spectrum, which resolved to an AB_2 system at an elevated temperature (353 K). When the sample was cooled to 223 K, two ABC spin systems were observed, because two rotamers of the compound are present in solution. The complexity of the dynamic processes prevented the extraction of detailed thermodynamic parameters by $^{31}P\{^1H\}$ VT NMR spectroscopy. Tris(phosphine) **H** was shown to act as a tridentate ligand forming square planar, tetrahedral, trigonal bipyramidal, and octahedral complexes with various metals (Pt, Cu, Fe, and Mo).

Tris(phosphine) **H** is somewhat similar to 1,8,9-trisubstituted anthracenes, in which the central atom (in position 9)

Received: May 1, 2016

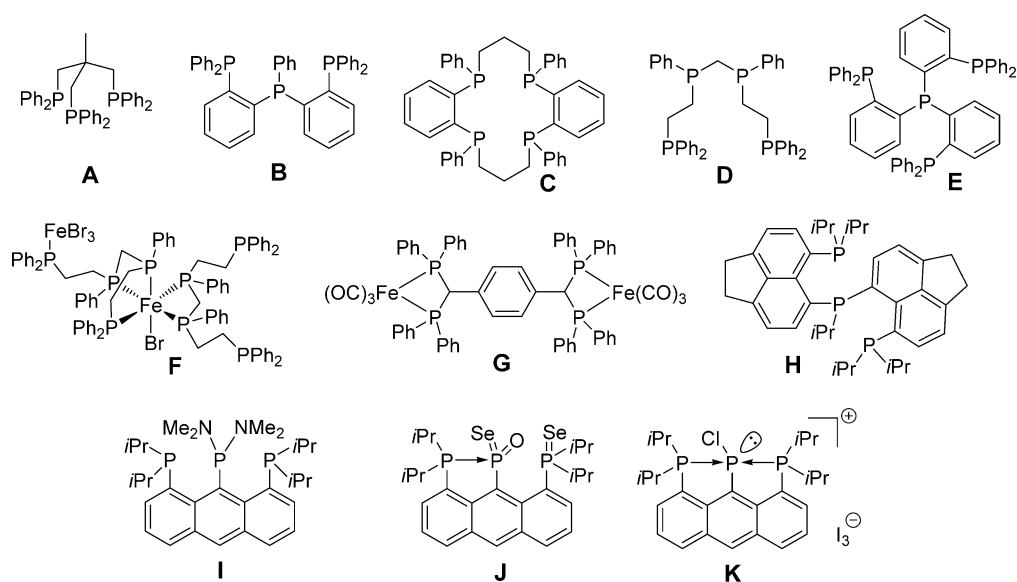
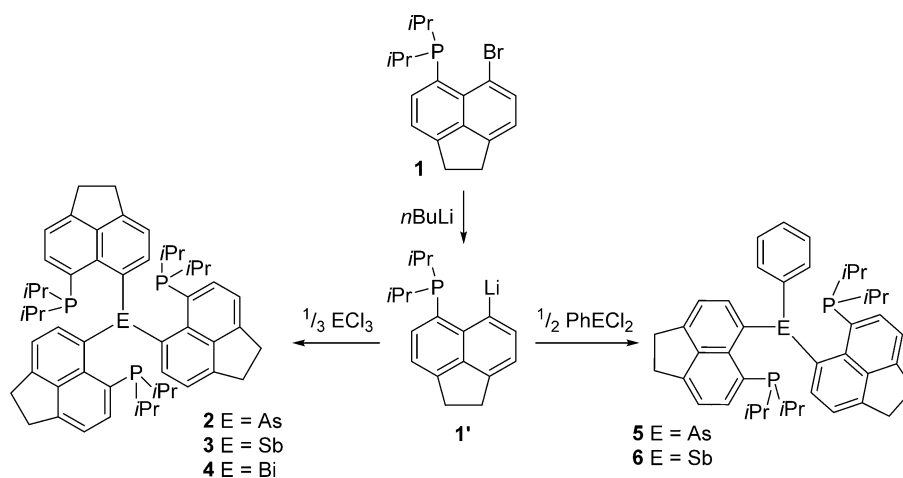


Figure 1. Selected literature examples of tri- and tetradentate phosphines (A–E), metal complexes (F and G), and 1,8,9-substituted anthracenes (I–K) discussed herein.

Scheme 1. Preparation of Compounds 2–6



also experiences two proximate *peri*-interactions. We have previously synthesized a short series of tris(phosphino)-anthracenes with a particular interest in their *peri*-region bonding and through-space interactions.⁹ Compound I shows no formal P–P bonding interaction, though it does show a remarkable $^{4\text{T}}J_{\text{PP}}$ of 104 Hz in an A_2M spin system. The Lewis base-stabilized *meta*-phosphonate (J) was synthesized from the reaction of I with methanol and selenium, and the double Lewis base stabilized phosphonium (K) was somehow unexpectedly synthesized by the reaction of I with P_2I_4 in 1,2-dichloroethane. While of high interest for their interesting bonding, several aspects make pnictogen 1,8,9-trisubstituted anthracenes rather challenging species with which to work. First, six synthetic steps are required in the preparation of I, starting from commercially available 1,8-dichloroanthraquinone.^{9,10} The yields at each step range between 51 and 93%, which means multigram quantities of I are not easily accessible. Another issue with 1,8,9-trisubstituted anthracenes species is that the central ring becomes dearomatized rather easily as shown by Hayes.¹¹ In a search for replacement of synthetically challenging 1,8,9-anthracenes, our attention turned to gemi-

nally bis(*peri*-substituted) pnictogens. These provide rather similar connectivity with respect to the central atom, which experiences two proximate *peri*-interactions. In contrast to the 1,8,9-trisubstituted anthracene manifold, the bis(*peri*-substituted) pnictogen platform provides additional angular flexibility as these molecules are not rigidly planar. Rather importantly, geminally bis(*peri*-substituted) species are synthetically much more viable. In this work, we report the synthesis and characterization of a bis(*peri*-substituted) arsine and stibine, which represent heavier homologues of ligand H. In addition, tris(*peri*-substituted) arsine, stibine, and bismuthine are reported; these represent the first examples of a new class of rigid tetradentate (P_3E) tris(*peri*-substituted) pnictine ligands.

RESULTS AND DISCUSSION

Syntheses. 5-Bromo-6-(diisopropylphosphino)acenaphthene (1) was used as the principal precursor in all syntheses described in this study.¹² The low-temperature lithium–halogen exchange reaction with *n*-butyllithium yielded 5-lithio-6-(diisopropylphosphino)acenaphthene (1'), which was, without isolation, subjected to C–E coupling with either

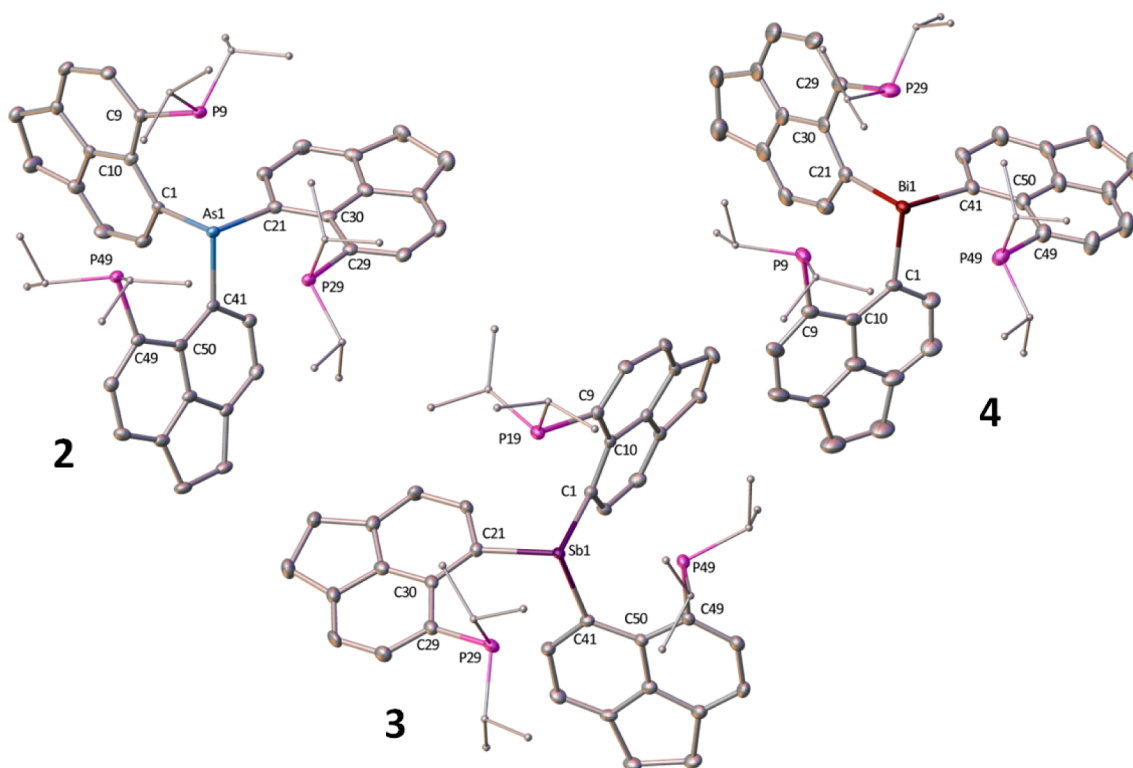


Figure 2. Crystal structures of 2–4. Solvating molecules (toluene for 3 and CH_2Cl_2 for 4) and hydrogen atoms have been omitted, with isopropyl groups simplified for the sake of clarity. Ellipsoids are plotted at the 40% probability level.

Table 1. Selected Bond Lengths, Displacements (angstroms), and Angles (degrees) for Compounds 2–6^a

	2	3·C ₇ H ₈	4·2CH ₂ Cl ₂	5·CH ₂ Cl ₂	6·2.5C ₇ H ₈
Distances					
C _{Ace} –P	1.846(3), –1.853(3)	1.832(6), –1.839(5)	1.80(2), –1.85(1)	1.837(7), –1.839(7)	1.837(2), –1.845(2)
C–E1	2.002(2), –2.021(3)	2.212(6), –2.224(5)	2.31(1), –2.34(1)	1.965(6), –2.003(7)	2.183(2), –2.214(2)
P···P	4.838(1), –5.251(1)	4.947(2), –5.484(2)	5.066(6), –5.484(5)	4.970(3)	5.2409(9)
P9···E1	3.2051(9)	3.305(1)	3.240(3) [3.279(4)]	3.120(2)	3.1684(7)
P29···E1	3.1938(8)	3.197(1)	3.250(4) [3.218(3)]	3.188(2)	3.2513(7)
P49···E1	3.162(1)	3.172(2)	3.250(3) [3.242(4)]	-	-
Angles					
C–E1–C	96.4(1), –98.7(1)	93.6(2), –97.3(2)	91.7(5), –96.0(5)	97.2(3), –100.0(3)	93.80(6), –96.04(6)
P···E1···P	98.91(2), –110.30(2)	99.59(4), –114.98(4)	103.3(1), –115.1(1)	103.97(5)	109.44(2)
splay angles ^b	16.5	10.1	15.9 [16.0]		
	15.5	15.2	15.9 [15.7]	15.2	14.1
	15.7	14.8	16.0 [16.0]	17.1	16.5
P–C···C–E1	15.5(1)	34.7(3)	2.8(7) [2.5(7)]		
	1.3(1)	0.0(3)	6.3(7) [1.5(7)]	0.5(4)	8.2(1)
	8.3(1)	0.1(3)	7.4(7) [8.6(8)]	9.3(4)	13.3(1)
Out-of-Plane Displacements					
P	0.139–0.391	0.194–0.599	0.025–0.338	0.102–0.211	0.041–0.216
E	0.197–0.273	0.197–0.881	0.027–0.442	0.194–0.314	0.379–0.431

^aValues in brackets are for the second molecule in the asymmetric unit. ^bThe splay angle equals the sum of the bay region angles – 360°.

$1/3$ molar equiv of ECl_3 (E = As, Sb, or Bi) or $1/2$ equiv of PhECl_2 (E = As or Sb) (Scheme 1). After aqueous workup under oxygen free conditions, novel compounds 2–6 were isolated as air sensitive white to yellow powders in moderate to high yields (32–80%). Compounds 2–6 are all hydrolytically stable and were fully characterized by multinuclear NMR spectroscopy (^1H , ^{13}C , and ^{31}P), single-crystal X-ray diffraction, mass spectrometry, and infrared and Raman spectroscopy, with the homogeneity confirmed by microanalysis.

Dichlorophenylarsine was prepared by the SO_2 reduction of phenylarsonic acid in the presence of HCl .¹³ Dichlorophenylstibine was prepared by the redistribution reaction of SbCl_3 and SbPh_3 .^{14,15} Multiple attempts to synthesize PhBiCl_2 via a related route resulted in the desired species being significantly contaminated by Ph_3Bi , Ph_2BiCl , and BiCl_3 , with purification by recrystallization from various solvents proving to be ineffective. The subsequent reaction of this impure material with **1'** resulted in complex, inseparable mixtures.

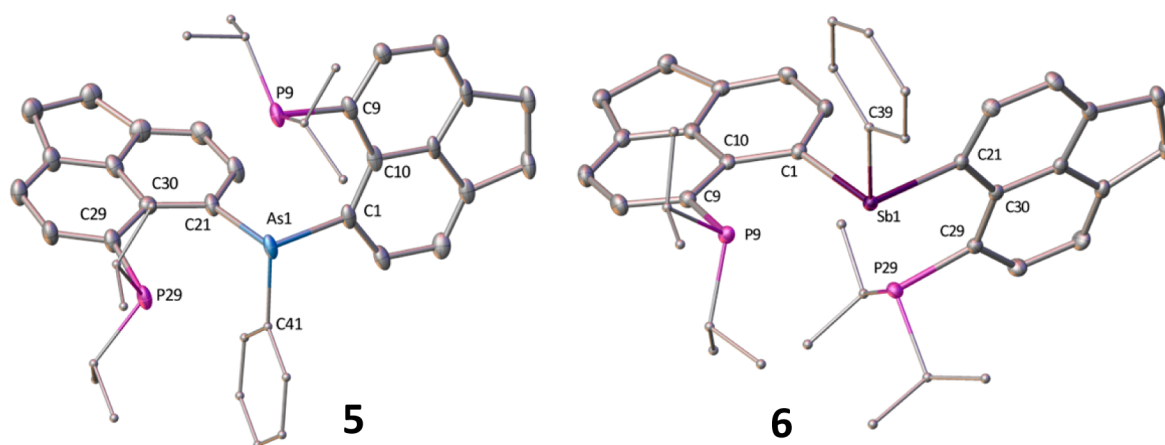


Figure 3. Crystal structures of **5** and **6**. Solvating molecules (CH_2Cl_2 for **5** and toluene for **6**) and hydrogen atoms have been omitted, with isopropyl and phenyl groups simplified for the sake of clarity. Ellipsoids are plotted at the 40% probability level.

While bis(*peri*-substituted) tridentate phosphine **H** has been prepared by the reaction of **1'** with $\frac{1}{2}$ molar equiv of $i\text{Pr}_2\text{P}(\text{Cl})_2$ cleanly with a good yield (68%),⁸ the low-temperature reaction of **1'** with $\frac{1}{3}$ molar equiv of PCl_3 gave a complex mixture of products (as judged by $^{31}\text{P}\{^1\text{H}\}$ NMR). Therefore, the tris(*peri*-substituted) phosphorus-centered congener of the series of **2**–**4** was deemed inaccessible by this route and was not pursued further.

Structural Investigations. Tris(acenaphthyl) Species 2–4. Crystal structures of compounds **2**–**4** are shown in Figure 2, with selected data listed in Table 1. In each case, the central pnictogen atom (As in **2**, Sb in **3**, and Bi in **4**) adopts a trigonal pyramidal geometry, with a slight increase in the acuteness of the $\text{C}_{\text{ipso}}-\text{E}-\text{C}_{\text{ipso}}$ angles following the As, Sb, Bi sequence (see Table 1). No strong dative interactions are formed between the Lewis basic $i\text{Pr}_2\text{P}$ groups and the central pnictogen atom as indicated by $\text{P}\cdots\text{E}$ distances, which range between 3.1 and 3.3 Å. The observed positive splay angles (10.1 – 16.5°) further support this notion. Despite three bulky *peri* groups being attached to the pnictogen centers in **2**–**4**, there are no major distortions of acenaphthene rings, with only moderate to medium in-plane and out-of-plane displacement of the *peri* atoms observed (Table 1). More significant deviations are observed only in one of the acenaphthene rings of **3**, which shows P and Sb out-of-plane displacements of 0.60 and 0.88 Å, with a corresponding $\text{P19}-\text{C9}\cdots\text{C1}-\text{Sb1}$ dihedral angle of $34.7(3)^\circ$. This is a significant increase versus those of the other two acenaphthene moieties in this molecule; however, this anomaly is readily explained through a local trade-off for decreased in-plane distortion in this particular *peri* motif that can be observed as a slightly diminished splay angle of 10.1° . For comparison, displacements in related singly acenaphthyl-substituted $i\text{Pr}_2\text{P}-\text{Ace}-\text{SbPh}_2$ are 0.111 and 0.039 Å, with a splay angle of $15.7(4)^\circ$.¹⁵

Because of the specifics of the *peri* substitution, all $\text{P}\cdots\text{E}$ distances are significantly sub-van der Waals [77–80% using van der Waals radii (R_{vdw}) values of 1.95 Å (P), 2.05 Å (As), 2.20 Å (Sb), and 2.30 Å (Bi)].¹⁶ If these short contacts were taken into account, the central pnictogen atom could also be viewed as attaining distorted octahedral geometry with its lone pair protruding through one of the octahedron faces. A collinear arrangement of all $\text{C}_{\text{ipso}}-\text{E}\cdots\text{P}$ motifs observed in the crystal structures of **2**–**4** is consistent with the onset of an $\text{n}(\text{P})\rightarrow\sigma^*(\text{E}-\text{C})$ $3\text{c}-4\text{e}$ interaction (see Figure 9).

Because of the large size and almost spherical shape of molecules **2**–**4**, the crystals have large voids that accommodate solvent easily. In all cases (except for one incidence of **2**), minor (unmodelled) disorder of the solvent was observed in the crystal structures.

Bis(acenaphthyl) Species 5 and 6. The crystal structures of **5** and **6** (Figure 3 and Table 1) show slight alleviation of the steric congestion around the central pnictogen atom (for **5**, E = As; for **6**, E = Sb) as one of the large $i\text{Pr}_2\text{P}-\text{Ace}$ units has been replaced with a phenyl ring.

As seen for the tris(acenaphthyl) species **2**–**4**, no strong dative interactions are present between the central pnictogen atoms and the $i\text{Pr}_2\text{P}$ groups, with $\text{P}\cdots\text{E}$ distances in the range of 3.12–3.25 Å. The arsenic and antimony atoms attain a trigonal pyramidal geometry. When sub-van der Waals contacts are taken into account, the As and Sb atoms display distorted tetragonal pyramidal geometry formed by three carbon atoms and two proximal $i\text{Pr}_2\text{P}$ groups, with the lone pair on the E atoms protruding through the base of the pyramid to complete the pseudo-octahedral coordination. There are no major distortions in either **5** or **6**, with the largest out-of-plane displacement being ~ 0.4 Å. The splay angles range between 14.1° and 17.1° ; also, the $\text{P}-\text{C}\cdots\text{C}-\text{E}$ dihedral angles compare well to the related parameters in compounds **2**–**4**. As described above, a collinear arrangement of all $\text{C}_{\text{ipso}}-\text{E}\cdots\text{P}$ motifs observed in crystal structures of **5** and **6** is consistent with the onset of an $\text{n}(\text{P})\rightarrow\sigma^*(\text{E}-\text{C})$ $3\text{c}-4\text{e}$ interaction. As in the crystal structures of **2**–**4**, in both **5** and **6**, solvent was incorporated into the crystal structure because of the large voids formed on packing.

NMR Spectroscopy. Tris(acenaphthyl) Species 2–4. Compounds **2**–**4** show sharp singlets at δ_{p} -13.0 (**2**), -19.1 (**3**), and -21.3 (**4**), indicating a slight increase in shielding of the phosphorus atoms on the descending group.¹⁵ Because of the crowded, propeller-like geometry of **2**–**4**, the ^1H and $^{13}\text{C}\{^1\text{H}\}$ NMR spectra display multiple anisochronous signals for chemically equivalent groups. Using **2** as an example, four CH_3 and two CH environments are observed as complex multiplets in the ^1H and $^{13}\text{C}\{^1\text{H}\}$ NMR spectra (Figure 5). The signals of methyl carbon atoms (δ_{C} 21.3–18.9) are second-order multiplets, corresponding to $\text{AA}'\text{A}''\text{X}$ spin systems (A = ^{31}P , and X = ^{13}C). Despite considerable effort, which included acquisition of the spectra at high field (16.4 T, 700 MHz instrument) and many iterative attempts, we have not been able

to simulate the spin systems to extract J couplings. This is because methyl carbons not only couple with ^{31}P atoms separated by two bonds ($^2J_{\text{CP}}$) but also have also non-negligible couplings with more distant phosphorus atoms. These two couplings, with a formal separation of 10 bonds ($^{10\text{TSS}}J_{\text{CP}}$), have different magnitudes, which results in a complex second-order signal. The shape of the signals is very sensitive to subtle changes in the coupling constants, which made the iterative fitting impossible. While we cannot determine the exact magnitude of these long-range couplings, we can confirm both these $^{10\text{TSS}}J_{\text{CP}}$ couplings are very likely non-negligible (i.e., >2 Hz) and different in each of the four diastereotopic methyl groups in 2–4. The through-bond component (through 10 bonds, ^{10}J) is likely to be very small, if not zero.¹⁷ Hence, it is highly likely that the couplings involve two through-space components (through two *peri* gaps); i.e., the magnetization is transferred due to the overlap of lone pairs on each of the two phosphorus atoms with the lone pair on the central arsenic atom (Figure 4).

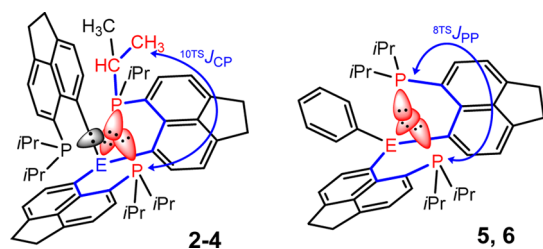


Figure 4. Graphical representation of the magnetization transfer pathway in long-range couplings. Bonds (formally) involved in the transfer are colored blue, and lone pairs involved in the transfer (through space) are colored red. The left panel shows one of the $^{10\text{TSS}}J_{\text{CP}}$ couplings between a CH_3 carbon atom and a distant P atom in molecules 2–4. The right panel shows $^{8\text{TSS}}J_{\text{PP}}$ coupling between the two P atoms in molecules 5 and 6.

In a similar vein, isopropyl CH environments (δ_{C} 26.8–25.8 in 2) display complex multiplets, corresponding to $\text{AA}'\text{A}''\text{X}$ spin systems (Figure 5).

Low-temperature (222 K) $^{31}\text{P}\{^1\text{H}\}$ NMR spectra of 2–4 did not display any observable line broadening or other notable changes, indicating no additional interlocking takes place at this temperature.

Bis(acenaphthyl) Species 5 and 6. The $^{31}\text{P}\{^1\text{H}\}$ NMR spectrum of 5 in d_8 -toluene (121.5 MHz, 298 K) shows two broad resonances at δ_{P} -11.5 and -14.4 (Figure 6). This is consistent with the molecule experiencing restricted rotational dynamics in solution, presumably around the $\text{As}-\text{C}_{\text{Acenap}}$ bonds [$\text{As}1-\text{C}1$ and $\text{As}1-\text{C}21$ (see Figure 3)]. In line with this, all signals in the ^1H NMR spectrum of 5 (298 K, 300.1 MHz) were broadened, while very broad signals were observed in the $^{13}\text{C}\{^1\text{H}\}$ NMR spectrum at the same temperature (75.5 MHz) (see the Supporting Information).

To gain insight into the dynamic behavior of 5, a variable-temperature NMR study was performed in the range of 223–373 K (Figure 6). When the sample of 5 was warmed to 373 K, a singlet was observed in the $^{31}\text{P}\{^1\text{H}\}$ NMR spectrum at δ_{P} -10.5 , indicating that the two phosphorus environments interchange rapidly at this temperature. When the sample was cooled to 223 K, the $^{31}\text{P}\{^1\text{H}\}$ NMR spectrum revealed two sharp doublets at δ_{P} -13.2 and -16.9 ($^{8\text{TSS}}J_{\text{PP}} = 11.5$ Hz), consistent with a simple AX spin system. The magnitude of

$^{8\text{TSS}}J_{\text{PP}}$ is remarkable because there is no direct overlap of the lone pairs on phosphorus atoms. The transfer of magnetization is highly likely to involve two through-space interactions because of the overlap of the two phosphorus lone pairs with the diffuse arsenic lone pair [$n(\text{P})\cdots n(\text{As})\cdots n(\text{P})$ interaction (Figure 4)].

Detailed line shape analysis of the $^{31}\text{P}\{^1\text{H}\}$ VT NMR spectra (see Figure S18 of the Supporting Information for the Eyring plot) yielded thermodynamic parameters of $\Delta H^\ddagger = 57.1$ kJ mol $^{-1}$ and $\Delta S^\ddagger = -17.5$ J mol $^{-1}$ K $^{-1}$ for the interchange process in 5. For completeness, the coalescence method gave a rotational barrier ΔG^\ddagger of 62.3 kJ mol $^{-1}$ at 340 K for 5. These data complement those obtained for the related tris-(phosphine) **H**, mentioned above. Because of the complexity of the dynamic processes in tris(phosphine) **H**, in which two ABC spin systems were present in the slow motion regime, the interchange process (equivalent to that described for 5) was masked, hence precluding determination of the exchange barrier through either line shape analysis or the coalescence method.

Compound 6 shows features similar to those of its arsenic homologue 5. The $^{31}\text{P}\{^1\text{H}\}$ NMR spectrum of 6 at 298 K (109.4 MHz) shows an extremely broad resonance (Figure 7). A variable-temperature NMR study revealed a sharp singlet (δ_{P} -17.5) at 363 K (fast motion regime) and two sharp doublets (δ_{P} -21.2 and -24.2) at 223 K (slow motion regime). The increased magnitude of $^{8\text{TSS}}J_{\text{PP}}$ between 5 and 6 (11.5 Hz vs 25.8 Hz, both at 223 K) can be attributed to the larger antimony atom acting as a more efficient mediator of magnetic spin information between the two phosphorus atoms (see Figure 4). The coalescence temperature of 6 was 303 K (at 109.4 MHz), which corresponds to a rotational barrier ΔG^\ddagger of 62.0 kJ mol $^{-1}$. This is remarkably similar to the energy barrier associated with interchange in 5, obtained from the detailed line shape analysis ($\Delta G^\ddagger = 62.4$ kJ mol $^{-1}$ at 303 K).

Computational Investigations. To complement these findings, we performed calculations at the B3LYP-D3/6-31G* level of density functional theory (DFT). Taking the arsenic compounds 2 and 5 as representatives, we optimized their structures starting from the single-crystal X-ray coordinates and subjected their wave functions were to natural bond orbital (NBO) analysis.¹⁸ The distances between the formally nonbonded As and P atoms are reasonably well reproduced at that level, e.g., for the mean $\text{As}\cdots\text{P}$ distance in 2 (DFT, 3.151 Å; X-ray, 3.189 Å).¹⁹ The localized lone pairs on phosphorus and arsenic atoms are visualized in Figure 8; these are somewhat “buried” within the molecules, in particular for tris(acenaphthyl) derivative 2, indicating they may not be readily available for coordination chemistry.

Arguably, there is repulsion between the lone pairs on As and P atoms. There are, however, weak attractions between these atoms counteracting this repulsion. In a second-order perturbation analysis, these are identified as $n(\text{P}) \rightarrow \sigma^*(\text{As}-\text{C}_{\text{ipso}})$ dative interactions worth approximately 10–11 kcal/mol each (for one of them, the relevant pair of NBOs is depicted in Figure 9). These interactions are likely to support the collinear arrangement of $\text{C}_{\text{ipso}}-\text{E}\cdots\text{P}$ motifs observed throughout the crystal structures of 2–5. These dative interactions give rise to notable Wiberg bond indices (WBIs) between the arsenic and phosphorus atoms, on the order of 0.10–0.11.²⁰ Slightly lower but still notable WBIs (approximately 0.07–0.09) and donor–acceptor energies (approximately 7–9 kcal/mol) are obtained at the same DFT level when the X-ray structures are employed

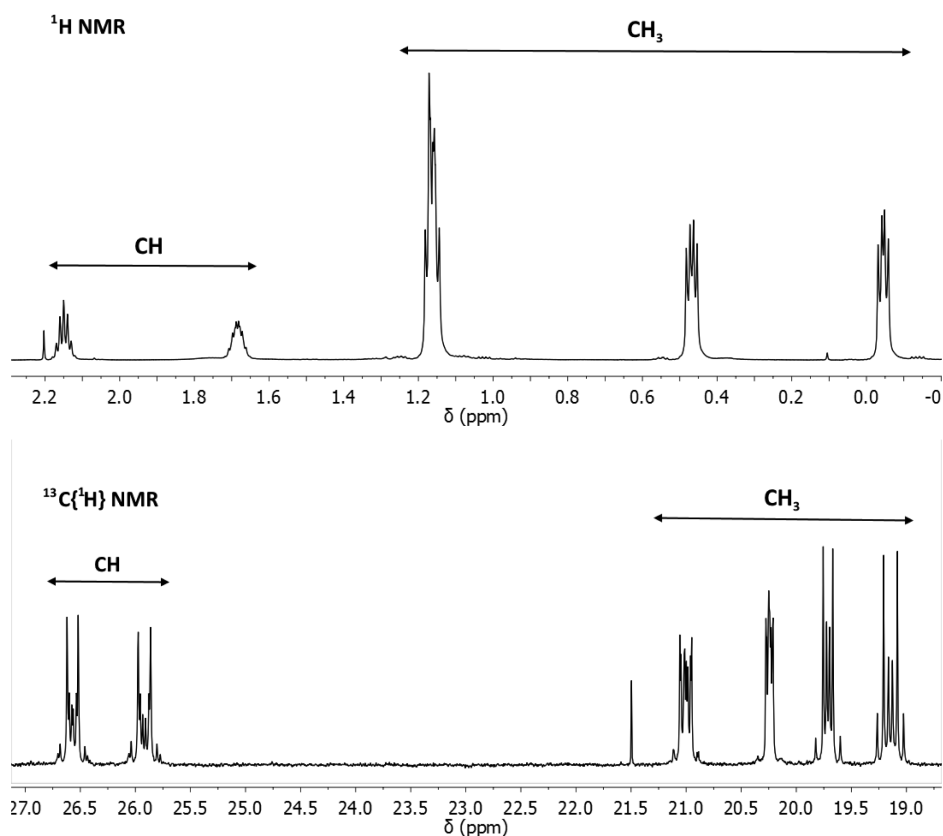


Figure 5. NMR spectra of **2**, the alkyl region of the ^1H NMR spectrum (recorded at 700.1 MHz) (top) and the alkyl region of the $^{13}\text{C}\{^1\text{H}\}$ NMR spectrum (recorded at 176.1 MHz) (bottom).

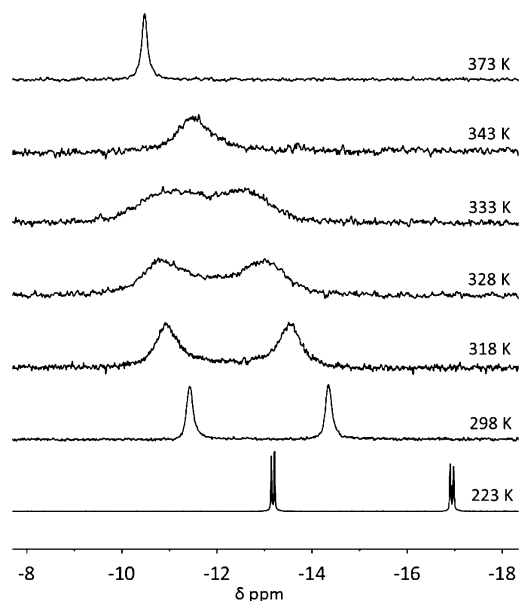


Figure 6. Variable-temperature $^{31}\text{P}\{^1\text{H}\}$ NMR spectra of **5** in d_8 -toluene at 121.5 MHz.

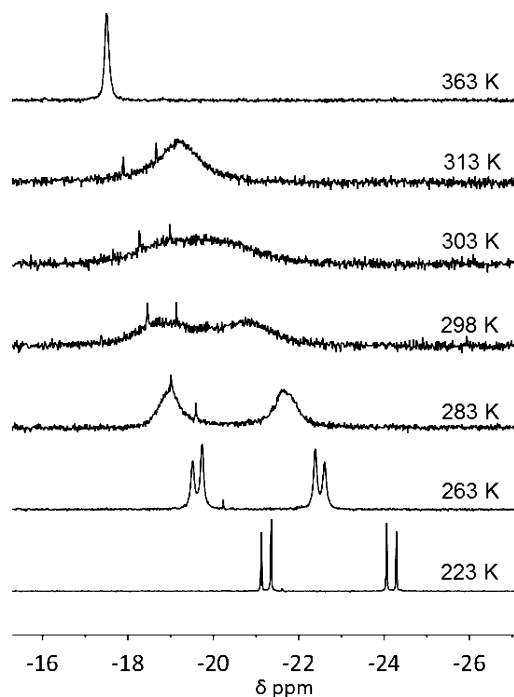


Figure 7. Variable-temperature $^{31}\text{P}\{^1\text{H}\}$ NMR spectra of **6** in d_8 -toluene at 109.4 MHz. Minor peaks are from an unrelated impurity.

without minimization. Similar characteristics have been found between other heavier chalcogen and pnictogen atoms in *peri*-naphthalene positions, where such notable dative interactions and WBIs have been taken as evidence of the onset of multicenter bonding.^{15,21,22}

CONCLUSION

Detailed structural and NMR spectroscopic study of bis-(phosphinoacenaphthyl) and tris(phosphinoacenaphthyl) pnict-

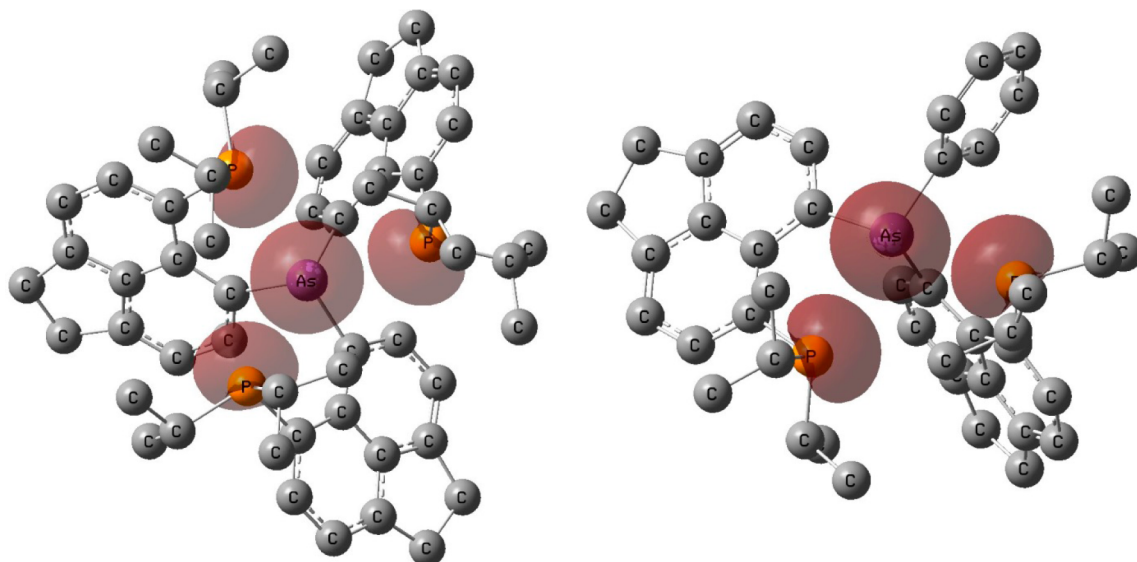


Figure 8. Plot of the lone pair NBOs in compounds **2** (left) and **5** (right). Hydrogen atoms have been omitted for the sake of clarity; isodensity values are 0.08 au. Molecules are viewed from “above” looking down the As lone pair; for other views, see the [Supporting Information](#).

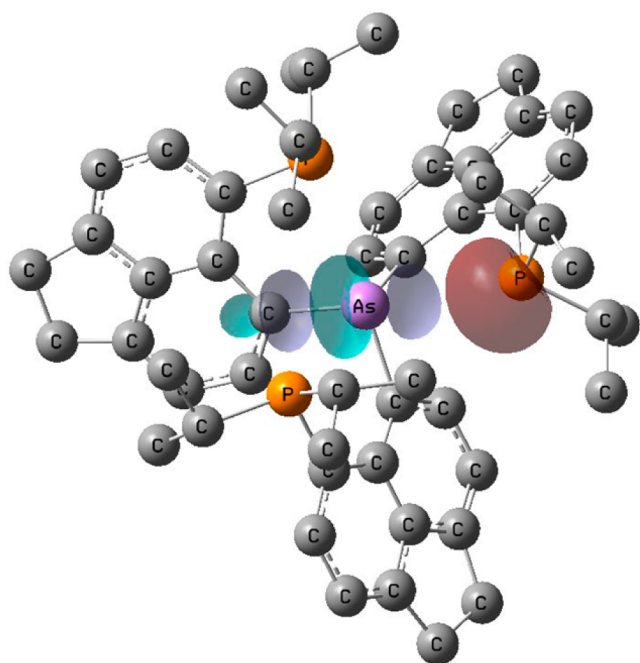


Figure 9. Plot of one pair of NBOs involved in dative interactions in **2**: red, lone pair donor on P; gray/turquoise, antibonding $\sigma^*(\text{As}-\text{C})$ acceptor orbital. H atoms have been omitted for the sake of clarity; isodensity values are 0.08 au.

tines confirmed the sterically crowded nature of these molecules, with sub-van der Waals P...E contacts across the *peri* region. However, relatively high yields and moderate acenaphthene ring distortions indicate that the blade-like arrangement of the substituents in these propeller-shaped molecules is rather accommodating. The relative simplicity of the $^{31}\text{P}\{^1\text{H}\}$ NMR spectra of **5** and **6** at low temperatures allowed determination of the long-range $^{8\text{TS}}J_{\text{PP}}$ couplings. Their magnitudes (11.5 and 25.8 Hz) are remarkable. The transfer of magnetization is likely to involve two through-space interactions in which the central pnictogen's lone pair acts as a “relay”; i.e., $n(\text{P})\cdots n(\text{E})\cdots n(\text{P})$ interactions (E = As or Sb)

take place. This is because the direct overlap of the two phosphorus atoms is ineffective, the P...P distances ranging from 4.838(1) to 5.484(5) Å (see [Table 1](#) and the plot of the lone pair NBOs in [Figure 8](#)). The lone pairs on the pnictogen atoms form a bowl-like environment, which, however, is somehow buried within the molecule. Coordination chemistry of these potential tetradentate (**2–4**) and tridentate (**5** and **6**) ligands will be studied next.

EXPERIMENTAL SECTION

General Considerations. All reactions and manipulations were performed under an atmosphere of nitrogen using standard Schlenk techniques or under an argon atmosphere in a Saffron glovebox. Dry solvents were either collected from an MBraun Solvent Purification System or dried according to common procedures.²³ Compound **1** was prepared according to the published procedure.¹² Antimony trichloride was purchased from Sigma-Aldrich and purified by vacuum sublimation before use. Dichlorophenylarsine (PhAsCl_2)¹³ and dichlorophenylstibine (PhSbCl_2)^{14,15} were prepared according to the published procedures; further details are in the [Supporting Information](#). Other chemicals were purchased from Acros Organics, Sigma-Aldrich, or Alfa Aesar and used as received. **Caution!** *Organoarsenic halides and arsenic halides are powerful vesicants, which cause severe irritation and blistering if allowed to come in contact with skin.* Suitable precautions, including the use of neoprene or rubber gloves when handling these, should be taken. Further experimental details are provided in the [Supporting Information](#).

Synthetic Methods. (*iPr*₂P-Ace)₃As (**2**). To a cooled (−78 °C) stirred solution of **1** (3.75 g, 10.7 mmol) in diethyl ether (100 mL) was added dropwise over 1 h *n*-butyllithium (4.30 mL, 2.5 M in hexanes, 10.7 mmol). The resulting solution was left to stir for a further 1 h at −78 °C. To this was added dropwise over 2 h a solution of arsenic trichloride (300 μL, 65 mg, 3.6 mmol) in diethyl ether (10 mL). The solution was left to warm to ambient temperature overnight. The volatiles were removed *in vacuo* and replaced with toluene (100 mL). The solution was washed with degassed water (45 mL) and the organic layer dried over magnesium sulfate. After filtration, the volatiles were again removed *in vacuo* to give a yellow powder (7.58 g, 80%) (mp >250 °C). Crystals suitable for X-ray diffraction work were grown from chloroform at room temperature. ¹H NMR ([Figure 10](#)) (700.1 MHz, CDCl₃): δ_{H} 7.62 (3H, dd, $^3J_{\text{HH}} = 7.1$ Hz, $^{7\text{TS}}J_{\text{HP}} = 1.7$ Hz, H-8), 7.57 (3H, d, $^3J_{\text{HH}} = 7.1$ Hz, H-2), 7.29 (3H, m, H-7), 6.86 (3H, d, $^3J_{\text{HH}} = 7.1$ Hz, H-3), 3.43–3.24 (12H, m, H-11,12), 2.15 (3H, h,

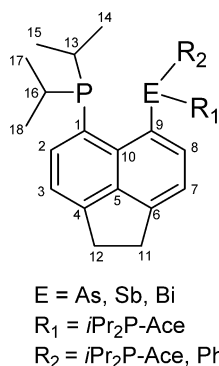


Figure 10. NMR numbering scheme for compounds 2–6.

³J_{HH} = 6.8 Hz, H-16), 1.72–1.65 (3H, m, H-13), 1.19–1.13 (18H, m, H-17,18), 0.47 (9H, dd, ³J_{HP} = 13.4 Hz, ³J_{HH} = 6.7 Hz, H-15), –0.04 (9H, dd, ³J_{HP} = 12.1 Hz, ³J_{HH} = 7.0 Hz, H-14). ¹³C{¹H} NMR (176.1 MHz, CDCl₃): δ_C 147.9 (s, qC-6), 145.7 (s, qC-4), 143.1–142.5 (m, ¹J_{CP} ≈ 49 Hz, qC-1), 141.0–140.7 (m, ~dt, ²J_{CP} ≈ 29 Hz, qC-10), 140.5 (s, C-2), 140.2–140.1 (m, qC-5), 133.8 (s, C-8), 132.4–132.0 (m, qC-9), 119.6 (s, C-3), 118.2 (s, C-7), 30.1 (s, C-11/12), 29.6 (s, C-11/12), 26.8–26.4 (m, C-16), 26.1–25.8 (m, C-13), 21.1–20.9 (m, C-18), 20.3–20.1 (m, C-17), 19.8–19.6 (m, C-14), 19.2–18.9 (m, C-15). ³¹P{¹H} NMR (202.5 MHz, CDCl₃): δ_P –13.0 (s). Infrared data (KBr disc, cm^{–1}): ν = 3021w (ν_{Ar–H}), 2921vs (ν_{C–H}), 1871m, 1607s, 1319s, 842vs. Raman data (glass capillary, cm^{–1}): ν = 3061m (ν_{Ar–H}), 2929s (ν_{C–H}), 1607s, 1561s, 1466s, 1412s, 1322vs, 580s. Elemental Anal. Calcd for C₅₄H₆₆P₃As: C, 73.46; H, 7.53. Found: C, 73.28; H, 7.45. HRMS (APCI+): *m/z* (%) calcd for C₅₄H₆₇P₃As 883.3666, found 883.3647 (100) [M + H⁺]; calcd for C₃₆H₄₄P₂As 613.2134, found 613.2109 (45) [M – *i*Pr₂P-Ace]; calcd for C₁₈H₂₃PAs 345.0753, found 345.0738 (5) [M – 2 × *i*Pr₂P-Ace + H].

(*i*Pr₂P-Ace)₃Sb (3). Compound 3 was prepared using the same procedure that was used for compound 2 except using 1 (3.00 g, 8.6 mmol) in diethyl ether (100 mL), *n*-butyllithium (3.4 mL, 2.5 M in hexanes, 8.6 mmol), antimony trichloride (650 mg, 2.9 mmol) in diethyl ether (8 mL), toluene (50 mL), and degassed water (25 mL), giving a yellow powder (2.46 g, 32%) (mp >250 °C). Crystals suitable for X-ray diffraction work were grown from toluene at –35 °C. ¹H NMR (500.1 MHz, CDCl₃): δ_H 7.85 (3H, d, ³J_{HH} = 6.6 Hz, H-2), 7.61 (3H, d, ³J_{HH} = 6.2 Hz, H-8), 7.29 (3H, d, ³J_{HH} = 7.3 Hz, H-7), 6.84 (3H, d, ³J_{HH} = 6.9 Hz, H-3), 3.40–3.25 (12H, m, H-11,12), 2.14 (3H, h, ³J_{HH} = 6.8 Hz, H-16), 1.88 (3H, dh, ²J_{HP} = 13.5 Hz, ³J_{HH} = 6.8 Hz, H-13), 1.21 (9H, m, H-18), 1.16 (9H, m, H-17), 0.56 (9H, m, H-14), 0.11 (9H, m, H-15). ¹³C{¹H} NMR (125.8 MHz, CDCl₃): δ_C 148.3 (s, qC-6), 145.7 (d, ¹J_{CP} = 57.6 Hz, qC-1), 145.2 (s, qC-4), 143.2 (s, C-2), 143.0–142.8 (m, qC-10), 140.0–139.8 (m, qC-5), 133.2 (s, C-8), 131.8–131.5 (m, qC-9), 120.2 (s, C-3), 118.2 (s, C-7), 30.2 (s, C-11/12), 29.9 (s, C-11/12), 27.1–26.8 (m, C-16), 25.6–25.4 (m, C-13), 21.0–20.8 (m, C-18), 20.0–19.9 (m, C-17), 19.8–19.7 (m, C-15), 19.6–19.5 (m, C-14). ³¹P NMR (202.5 MHz, CDCl₃): δ_P –19.1 (s). Infrared data (KBr disc, cm^{–1}): ν = 3024w (ν_{Ar–H}), 2922vs, 2864vs (ν_{C–H}), 1604s, 1587s, 1461s, 1320s. Raman data (glass capillary, cm^{–1}): ν = 3059m (ν_{Ar–H}), 2926vs (ν_{C–H}), 2870s (ν_{C–H}), 1321vs, 579s. Elemental Anal. Calcd for C₅₄H₆₆P₃Sb: C, 69.76; H, 7.15. Found: C, 69.63; H, 7.27. HRMS (APCI+): *m/z* (%) calcd for C₅₄H₆₇P₃Sb 929.3488, found 929.3496 (12) [M + H⁺]; calcd for C₃₆H₄₄P₂Sb 659.1951, found 659.1956 (100) [M – *i*Pr₂P-Ace].

(*i*Pr₂P-Ace)₃Bi (4). To a cooled (–78 °C) rapidly stirred solution of 1 (1.00 g, 2.86 mmol) in diethyl ether (25 mL) was added dropwise over 30 min *n*-butyllithium (1.2 mL, 2.5 M in hexanes, 2.95 mmol). The resulting yellow suspension was stirred for 3 h at this temperature. A cooled (–78 °C) suspension of BiCl₃ (296 mg, 0.94 mmol) in diethyl ether (30 mL) was prepared and stirred rapidly. The first suspension was added via cannula to the BiCl₃ with the mixture being stirred for 1.5 h at this temperature. The reaction mixture was allowed to warm to ambient temperature overnight, resulting in a

white precipitate that was collected via filtration. The solid was washed with diethyl ether (2 × 10 mL) and then degassed water (10 mL) and dried *in vacuo* for 4 h. The product was obtained as a white powder (300 mg, 0.29 mmol, 32%) (mp 202–203 °C dec). X-ray quality crystals of 4 were grown from a saturated solution in dichloromethane at 0 °C. ¹H NMR (500.1 MHz, CDCl₃): δ_H 8.60 (3H, dd, ³J_{HH} = 6.9 Hz, ⁷s_J_{HP} = 2.4 Hz, H-8), 7.60 (3H, dd, ³J_{HH} = 7.2 Hz, ³J_{HP} = 2.8 Hz, H-2), 7.27 (3H, d, ³J_{HH} = 7.1 Hz, H-3), 6.85 (3H, d, ³J_{HH} = 6.8 Hz, H-7), 3.38–3.19 (12H, m, H11/12), 2.10 (3H, h, ³J_{HH} = 6.9 Hz, H-16), 1.89 (3H, h, ³J_{HH} = 6.8 Hz, H-13), 1.22 (9H, dd, ~q, ³J_{HP} = 13.4 Hz, ³J_{HH} = 7.0 Hz, H-17), 1.12 (9H, dd, ~q, ³J_{HP} = 10.1 Hz, ³J_{HH} = 6.9 Hz, H-18), 0.63 (9H, dd, ~q, ³J_{HP} = 14.4 Hz, ³J_{HH} = 6.8 Hz, H-14), 0.17 (9H, dd, ~q, ³J_{HP} = 12.6 Hz, ³J_{HH} = 6.9 Hz, H-15). ¹³C NMR (125.8 MHz, CDCl₃): δ_C 176.6 (s, qC-9), 148.8 (s, qC-4), 146.6 (s, C-8), 145.3–144.9 (m, qC-10), 144.0 (s, qC-6), 141.5–141.3 (m, qC-5), 132.7 (s, C-2), 132.6–132.4 (m, qC-1), 123.5 (s, C-7), 117.9 (s, C-3), 130.2 (s, C-11/12), 130.1 (s, C-11/12), 27.0–26.7 (m, C-16), 25.5–25.3 (m, C-13), 21.5–21.2 (m, C-18), 20.3–20.1 (m, C-17), 19.9–19.5 (m, C14,15). ³¹P{¹H} NMR (202.5 MHz, CDCl₃): δ_P –21.3 (s). Infrared data (KBr disc, cm^{–1}): ν = 3022w (ν_{Ar–H}), 2948s (ν_{C–H}), 1631br, 1460s, 1322s, 1245s. Raman data (glass capillary, cm^{–1}): ν = 3048m (ν_{Ar–H}), 1570m, 999s, 211s. Elemental Anal. Calcd for C₅₄H₆₆P₃Bi: C, 63.77; H, 6.46. Found: C, 63.64; H, 6.46. HRMS (APCI+): *m/z* (%) calcd for C₅₄H₆₇P₃Bi 1017.4244, found 1017.4254 [M + H⁺].

(*i*Pr₂P-Ace)₂AsPh (5). To a cooled (–78 °C), rapidly stirring solution of 1 (3.00 g, 8.6 mmol) in diethyl ether (75 mL) was added over a period of 1 h *n*-butyllithium (3.5 mL, 2.5 M solution in hexanes, 8.6 mmol), and the mixture was left to stir for 2 h at the same temperature. A solution of dichlorophenylarsine (0.96 g, 0.58 mL, 4.6 mmol) in diethyl ether (10 mL) was added dropwise over 1 h and the resulting solution left to warm to ambient temperature overnight. Additional diethyl ether (110 mL) was added, along with degassed water (25 mL), and the solution was stirred vigorously for 10 min. The organic layer was separated and dried over magnesium sulfate. The volatiles were removed *in vacuo* to give a yellow powder that was dried *in vacuo* for 3 h (1.91 g, 64%) (mp 160 °C). X-ray quality crystals of 5 were grown from dichloromethane at –35 °C. ¹H NMR (300.1 MHz, *d*₈-toluene, 298 K): δ_H 7.76 (br s), 7.56 (br s), 7.59 (br s), 6.93 (br s), 6.75 (br s), 2.97 (br s, H-11,12), 2.47 (br s), 2.16 (br s), 1.98 (br s), 1.85 (br s), 1.51 (3H, br s, 1 × CH₃), 1.46 (3H, br s, 1 × CH₃), 1.29 (3H, br s, 1 × CH₃), 1.09 (3H, br s, 1 × CH₃), 1.03 (3H, br s, 1 × CH₃), 0.57 (3H, br s, 1 × CH₃), 0.33 (3H, br s, 1 × CH₃), 0.15 (3H, br s, 1 × CH₃). ¹H NMR (300.1 MHz, *d*₈-toluene, 223 K): δ_H 8.19 (1H, d, ³J_{HH} = 7.2 Hz, H-8), 7.90 (1H, dd, ³J_{HH} = 7.2 Hz, ³J_{HP} = 2.2 Hz, H-2), 7.66 (1H, d, ³J_{HH} = 7.1 Hz, H-8'), 7.61 (1H, dd, ³J_{HH} = 7.2 Hz, ³J_{HP} = 3.1 Hz, H-2'), 7.54 (1H, dd, ³J_{HH} = 7.3 Hz, ³J_{HP} = 3.0 Hz, H-21), 7.51 (1H, d, ³J_{HH} = 7.5 Hz, H-20), 7.40 (1H, pseudo dd, ³J_{HH} = 7.5 Hz, H-22), 7.22–7.15 (2H, m, H-20',21'), 7.05–6.99 (2H, m, H-3',7'), 6.96 (1H, d, ³J_{HH} = 7.2 Hz, H-3), 6.79 (1H, d, ³J_{HH} = 7.2 Hz, H-7), 3.08–2.85 (8H, m, H-11,11',12,12'), 2.51 (1H, h, ³J_{HH} = 7.0 Hz, H-13), 1.95 (1H, h, ³J_{HH} = 6.8 Hz, H-13'), 2.16 (1H, br s, H-16), 1.84 (1H, h, ³J_{HH} = 6.7 Hz, H-16'), 1.56 (3H, dd, ³J_{HP} = 12.6 Hz, ³J_{HH} = 7.2 Hz, 1 × CH₃), 1.50 (3H, dd, ³J_{HP} = 11.5 Hz, ³J_{HH} = 6.9 Hz, 1 × CH₃), 1.13–1.04 (6H, m, 2 × CH₃), 0.61 (3H, dd, ³J_{HP} = 15.7 Hz, ³J_{HH} = 6.6 Hz, 1 × CH₃), 0.35 (3H, dd, ³J_{HP} = 13.2 Hz, ³J_{HH} = 6.8 Hz, 1 × CH₃), 0.22 (3H, ³J_{HP} = 13.5 Hz, ³J_{HH} = 6.7 Hz, 1 × CH₃). ¹³C{¹H} NMR (75.5 MHz, *d*₈-toluene, 298 K): no signals were observed due to extreme broadening. ¹³C{¹H} NMR (75.5 MHz, *d*₈-toluene, 223 K): low solubility prevented acquisition of the spectrum. ³¹P{¹H} NMR (162.0 MHz, *d*₈-toluene, 293 K): δ_P –11.6 (s), –14.4 (s). ³¹P{¹H} NMR (162.0 MHz, *d*₈-toluene, 223 K): δ_P –13.2 (d, ⁸s_J_{PP} = 11.5 Hz), –16.9 (d, ⁸s_J_{PP} = 11.5 Hz). ³¹P{¹H} NMR (162.0 MHz, *d*₈-toluene, 373 K): δ_P –10.5 (s). Infrared data (KBr disc, cm^{–1}): ν = 3064w (ν_{Ar–H}), 2947vs (ν_{C–H}), 1872m, 1460s, 1319s, 840s, 736s. Raman data (glass capillary, cm^{–1}): ν = 3066m (ν_{Ar–H}), 2948s (ν_{C–H}), 1607s, 1564s, 1445s, 1322vs, 582s. Elemental Anal. Calcd (%) for C₄₂H₄₉P₂As·1/2CH₂Cl₂: C, 69.62; H, 6.87. Found: C, 69.61; H, 6.62. HRMS (APCI+): *m/z* (%) calcd for C₄₂H₅₀P₂As 691.2598, found 691.2604 (10) [M + H⁺]; calcd for C₃₆H₄₄P₂As 613.2129, found

613.2127 (55) [M – Ph]; calcd for C₁₈H₂₂PAs 421.1066, found 421.1060 (100) [M – iPr₂P-Ace].

(iPr₂P-Ace)₂SbPh (6). Compound 6 was prepared using the same procedure as per compound 5 using 1 (1.00 g, 2.90 mmol) in diethyl ether (30 mL), *n*-butyllithium (1.1 mL, 2.5 M in hexanes, 2.90 mmol), dichlorophenylstibine (390 mg, 1.45 mmol) in diethyl ether (20 mL), additional diethyl ether (25 mL), and degassed water (10 mL), giving a yellow powder (1.63 g, 77%) (mp 165–167 °C). Crystals suitable for X-ray diffraction work were grown from toluene under ambient conditions. ¹H NMR (500.1 MHz, *d*₈-toluene, 298 K): δ_H 8.02 (1H, d, ³J_{HH} = 7.0 Hz), 7.86–7.78 (m), 7.56 (dd, ³J_{HH} = 7.1 Hz, ³J_{HP} = 3.5 Hz), 7.20–7.06 (m), 6.75 (br s), 7.02 (br s), 6.99 (br s), 6.83 (br s), 2.99 (br s, H-11,12), 2.13–2.06 (m), 2.16 (br s), 2.08–1.88 (m), 1.59–0.08 (12H, v. br s, 8 × CH₃). ¹H NMR (400.1 MHz, *d*₈-toluene, 223 K): δ_H 8.16 (12H, v. br s, 8 × CH₃), 7.56 (br s), 7.47 (br s), 7.28–6.87 (br m), 3.06–2.77 (br s, H-11,12), 2.24–2.07 (br s, H-13), 2.00–1.82 (br s, H-13), 1.47 (3H, dd, ³J_{HP} = 14.7 Hz, ³J_{HH} = 7.1 Hz, 1 × CH₃), 1.37–0.99 (6H, m, 2 × CH₃), 0.73 (3H, dd, ³J_{HP} = 15.6 Hz, ³J_{HH} = 6.9 Hz, 1 × CH₃), 0.53 (3H, dd, ³J_{HP} = 14.0 Hz, ³J_{HH} = 6.9 Hz, 1 × CH₃), 0.20 (3H, dd, ³J_{HP} = 14.1 Hz, ³J_{HH} = 7.1 Hz, 1 × CH₃). ¹³C{¹H} NMR (75.5 MHz, *d*₈-toluene, 298 K): no signals were observed due to extreme broadening. ¹³C{¹H} NMR (75.5 MHz, *d*₈-toluene, 223 K): low solubility prevented acquisition of the spectrum. ³¹P{¹H} NMR (162.0 MHz, *d*₈-toluene, 298 K): δ_P –17.2 to –22.2 (v. br s). ³¹P{¹H} NMR (109.4 MHz, *d*₈-toluene, 363 K): δ_P –17.5 (s). ³¹P{¹H} NMR (109.4 MHz, *d*₈-toluene, 223 K): δ_P –21.2 (d, ⁸sJ_{PP} = 25.8 Hz), –24.2 (d, ⁸sJ_{PP} = 25.8 Hz). Infrared data (KBr disc, cm^{–1}): ν = 3057m (ν_{Ar–H}), 2922vs (ν_{C–H}), 2824vs (ν_{C–H}), 1601s, 1461s, 1247s, 844s. Raman data (glass capillary, cm^{–1}): ν = 3049m (ν_{Ar–H}), 2928m (ν_{C–H}), 2858m (ν_{C–H}), 1603m, 1328vs. Elemental Anal. Calcd (%) for C₄₂H₄₉P₂Sb: C, 68.40; H, 6.70. Found: C, 68.35; H, 6.76. HRMS (APCI+): *m/z* (%) calcd for C₄₂H₅₀P₂Sb 737.2420, found 737.2415 (65) [M + H⁺]; calcd for C₃₆H₄₄P₂Sb 659.1956, found 659.1945 (100) [M – Ph].

X-ray Diffraction. The crystallographic details relating to this work can be found in the [Supporting Information](#). CCDC 1476664–1476668 contain the crystallographic data for this paper. These data can be obtained free of charge from The Cambridge Crystallographic Data Centre via www.ccdc.cam.ac.uk/data_request/cif. Multiple data collections of all samples (2–6) were conducted, with crystals grown from a variety of solvents. The best quality data sets were used for refinements. In all but one case (2), solvent was incorporated into the crystals. Because of the close-to-spherical shape of molecules 2–6, the incorporation of disordered solvent into the crystals could not be prevented. Although some of the crystal data sets appear to be of lower quality upon first inspection, they are sufficient to demonstrate the connectivity for the purposes of this work.

■ ASSOCIATED CONTENT

● Supporting Information

The Supporting Information is available free of charge on the [ACS Publications website](#) at DOI: [10.1021/acs.inorgchem.6b01079](https://doi.org/10.1021/acs.inorgchem.6b01079).

Further synthetic details, NMR spectra of compounds 2–6, ³¹P{¹H} VT NMR spectra of 5 and 6 (including the Eyring plot for 5), further X-ray diffraction details, additional computational details, and coordinates of the DFT-optimized structures ([PDF](#))
Crystallographic data ([CIF](#))

■ AUTHOR INFORMATION

Corresponding Author

*E-mail: pk7@st-andrews.ac.uk.

Notes

The authors declare no competing financial interest.

■ ACKNOWLEDGMENTS

This work was financially supported by the EPSRC and COST actions CM0802 PhoSciNet and SM1302 SIPs. The authors thank the University of St Andrews NMR Service and the EPSRC UK National Mass Spectrometry Facility at Swansea University (NMSF).

■ REFERENCES

- (1) Broda, H.; Hinrichsen, S.; Tuzcek, F. *Coord. Chem. Rev.* **2013**, *257*, 587.
- (2) Pascariu, A.; Iliescu, S.; Popa, A.; Ilia, G. *J. Organomet. Chem.* **2009**, *694*, 3982.
- (3) Hewertson, W.; Watson, H. R. *J. Chem. Soc.* **1962**, 1490.
- (4) Hartley, J. G.; Venanzi, L. M.; Goodall, D. C. *J. Chem. Soc.* **1963**, 3930.
- (5) Kyba, E. P.; Hudson, C. W.; McPhaul, M. J.; John, A. M. *J. Am. Chem. Soc.* **1977**, *99*, 8053.
- (6) Jana, B.; Hovey, M.; Ellern, A.; Pestovsky, O.; Sadow, A. D.; Bakac, A. *Dalton Trans.* **2012**, *41*, 12781.
- (7) Barney, A. A.; Fanwick, P. E.; Kubiak, C. P. *Organometallics* **1997**, *16*, 1793.
- (8) Ray, M. J.; Randall, R. A. M.; Athukorala Arachchige, K. S.; Slawin, A. M. Z.; Bühl, M.; Lébl, T.; Kilian, P. *Inorg. Chem.* **2013**, *52*, 4346.
- (9) Kilian, P.; Slawin, A. M. Z. *Dalton Trans.* **2007**, 3289.
- (10) Yamashita, M.; Watanabe, K.; Yamamoto, Y.; Akiba, K. *Chem. Lett.* **2001**, 1104.
- (11) Ritch, J. S.; Julienne, D.; Rybchinski, S. R.; Brockman, K. S.; Johnson, K. R. D.; Hayes, P. G. *Dalton Trans.* **2014**, *43*, 267.
- (12) Wawrzyniak, P.; Fuller, A. L.; Slawin, A. M. Z.; Kilian, P. *Inorg. Chem.* **2009**, *48*, 2500.
- (13) Adams, E.; Jeter, D.; Cordes, A. W.; Kolis, J. W. *Inorg. Chem.* **1990**, *29*, 1500.
- (14) Herrmann, W. A.; Karsch, H. H. *Synthetic Methods of Organometallic and Inorganic Chemistry Volume 3: Phosphorus, Arsenic, Antimony and Bismuth*; Thieme: New York, 1996; Vol. 3.
- (15) Chalmers, B. A.; Bühl, M.; Athukorala Arachchige, K. S.; Slawin, A. M. Z.; Kilian, P. *Chem. - Eur. J.* **2015**, *21*, 7520.
- (16) Batsanov, S. S. *Inorg. Mater.* **2001**, *37*, 871.
- (17) Hierso, J.-C. *Chem. Rev.* **2014**, *114*, 4838.
- (18) Reed, A. E.; Curtiss, L. A.; Weinhold, F. *Chem. Rev.* **1988**, *88*, 899.
- (19) Note that empirical dispersion corrections are instrumental for reaching this good agreement; at the standard B3LYP/6-31G* level, the P–As bond distances are significantly overestimated (e.g., mean value of 3.306 Å in 2).
- (20) Wiberg, K. B. *Tetrahedron* **1968**, *24*, 1083.
- (21) Nordheider, A.; Hupf, E.; Chalmers, B. A.; Knight, F. R.; Bühl, M.; Mebs, S.; Chęcińska, L.; Lork, E.; Camacho, P. S.; Ashbrook, S. E.; Athukorala Arachchige, K. S.; Cordes, D. B.; Slawin, A. M. Z.; Beckmann, J.; Woollins, J. D. *Inorg. Chem.* **2015**, *54*, 2435.
- (22) Knight, F. R.; Diamond, L. M.; Athukorala Arachchige, K. S.; Sanz Camacho, P.; Randall, R. A. M.; Ashbrook, S. E.; Bühl, M.; Slawin, A. M. Z.; Woollins, J. D. *Chem. - Eur. J.* **2015**, *21*, 3613.
- (23) Armarego, W. L. F.; Chai, C. L. L. *Purification of Laboratory Chemicals*, 6th ed.; Elsevier: Burlington, MA, 2009.